Araştırma Makalesi
Adıyaman Üniversitesi Mühendislik Bilimleri Dergisi
22 (2024) 35-45

THE EFFECTS OF LASER MICRO-ENGRAVING VARIABLES ON THE SURFACE CHARACTERISTICS OF THE Ti-6Al-7Nb ALLOY

Sertan OZAN[1]*

[1]Yozgat Bozok Üniversitesi, Mühendislik-Mimarlık Fakültesi, Makine Mühendisliği Bölümü, Yozgat, 66100, Türkiye
Geliş Tarihi/Received Date: 25.11.2023 Kabul Tarihi/Accepted Date: 26.03.2024 DOI: 10.54365/adyumbd.1395281

ABSTRACT

This investigation aims to analyze the impact of scanning direction, scanning speed, and power level (%) on the surface roughness of Ti-6Al-7Nb alloy specimens subjected to laser micro-engraving. The laser micro-engraving process was carried out by scanning the predetermined geometric configuration six times. Factorial analysis was implemented to determine the impact of system parameters on the surface roughness. Throughout the micro-engraving operations, line spacing, frequency, and pulse width parameters were maintained at a consistent value of 0.03 mm, 100 kHz, and 300 ns, respectively. The optimal conditions for achieving the lowest surface roughness were observed at a scanning speed of 700 mm/s, a power level of 60%, and a scanning direction of 90°. Moreover, in accordance with the experimental parameters employed in this investigation, it was observed that increasing the scanning speed while maintaining a constant power level (%) reduced surface roughness. There was a direct correlation between the increase in power level (%) and a corresponding increase in surface roughness.

Keywords: *Laser, micro-engraving, Ti-6Al-7Nb alloy, surface roughness*

LAZER MİKRO-OYMA DEĞİŞKENLERİNİN Ti-6Al-7Nb ALAŞIMININ YÜZEY ÖZELLİKLERİ ÜZERİNE ETKİLERİ

ÖZET

Bu araştırma, lazer mikro-oyma işlemine tabi tutulan Ti-6Al-7Nb alaşım numunelerinin yüzey pürüzlülüğü üzerinde tarama yönünün, tarama hızının ve lazer gücünün (%) etkisini analiz etmeyi amaçlamaktadır. Lazer oyma işlemi, önceden belirlenmiş geometrik konfigürasyonun altı kez taranmasıyla gerçekleştirildi. Sistem parametrelerinin yüzey pürüzlülüğü üzerindeki etkisini belirlemek için faktöriyel analiz uygulanmıştır. Mikro-oyma işlemleri boyunca tarama aralığı, frekans ve atım genişliği parametreleri sırasıyla 0,03 mm, 100 kHz ve 300 ns'lik bir değerde tutulmuştur. En düşük yüzey pürüzlülüğüne ulaşmak için en uygun koşullar, 700 mm/s tarama hızında, %60 güç seviyesinde ve 90° tarama yönünde gözlemlendi. Ayrıca, bu araştırmada kullanılan deneysel parametrelere uygun olarak, sabit bir güç seviyesi (%) korunurken tarama hızının arttırılmasının yüzey pürüzlülüğünü azalttığı gözlemlenmiştir. Güç seviyesindeki artış (%) ile yüzey pürüzlülüğündeki buna karşılık gelen artış arasında doğrudan bir ilişki tespit edilmiştir.

Anahtar Kelimeler: *Lazer, mikro-oyma, Ti-6Al-7Nb alaşımı, yüzey pürüzlülüğü*

1. Introduction

In the contemporary landscape of intense market competition, enterprises heavily depend on state-of-the-art manufacturing technology to achieve elevated production efficiency levels while upholding product quality standards [1, 2]. Furthermore, the prevailing inclination towards reducing the size of products requires the advancement of novel micro- and nano-manufacturing technologies [3].

Micro-processing with industrial lasers is utilized to meet the requirements of intricate and precise geometries; it is general knowledge that accurate tool action and machining strategy are required for

* e-posta[1] : sertan.ozan@bozok.edu.tr ORCID ID: https://orcid.org/0000-0003-1932-8308 (Sorumlu Yazar)

intricate details [4]. Laser beam-aided machining (LAM) is a thermal energy-based machining process that operates without physical contact and is capable of being utilized on a diverse array of materials [5]. Concentrating the laser beam to the point where the excess material is melted and vaporized from the parent material can precisely form a gravure through many overlapped microscopic cavities in the metal surface [5]. Instead of the material's mechanical properties, the thermal and optical qualities play a role in this method; laser machining works best with hard materials and materials exhibiting low conductivity and thermal diffusivity [5].

LAM is used for various operations, including milling, engraving, turning, drilling, and grooving. These applications each make use of their one-of-a-kind strategy for the removal of material [6]. In LAM, there are three processes involved in the removal of materials: (1) melting, (2) vaporization, and (3) chemical degradation [6]. The basic machining procedure in laser beam micro-engraving is based on creating grooves with many overlapped craters by evaporating the material in the interaction area according to a strategy [3, 7]. The procedure relies on removing many layers that are requisite to achieve the intended depth; the depth of micro-engraving is determined by the number of layers created by overlapping and spreading parallel grooves over the surface using a specific scanning strategy, as well as the amount of evaporated material [7]. Removal rates exceeding fractions of mm^3/s and surface quality equivalent to chip removal-based procedures distinguish laser-based micro-milling [7].

Many industries use titanium alloys, including the aerospace [8-10] and medical sectors [11-13]. The utilization of titanium alloys in biomedical implants to repair hard tissues is highly sought after due to their exceptional resistance to corrosion, biocompatibility, and strength [14-16]. Titanium and its alloys not only have low thermal conductivity but also demonstrate significant chemical reactivity, particularly with the materials employed in cutting tools [17]. A robust adhesion phenomenon exists at the interface between the tool and chip, as well as at the contact point between the tool and workpiece material, combined with a high cutting temperature; it can cause problems during machining, and cutting tools wear extremely rapidly [17]. In addition, titanium and its alloys are tricky to mill; hence, their machining is sometimes seen as a severe challenge [17-20].

The biomedical sector extensively uses Ti-6Al-4V alloy because of its excellent tensile strength-to-weight ratio and superior corrosion resistance [21, 22]. Notably, anti-corrosion and wear-resistant vanadium-free titanium alloys for orthopedic implant devices have been developed due to worries about potentially harmful vanadium ions from the Ti-6Al-4V alloy [23]. To generate a more biocompatible titanium alloy for biomedical applications, niobium was substituted for vanadium in Ti-6Al-4V to form Ti6Al-7Nb [24]. Compared to the extensively researched Ti-6Al-4V alloy, the Ti-6Al-7Nb alloy has received significantly less attention [25]. This study explores the feasibility of using a laser beam to engrave narrow and complex geometries on the surface of Ti6Al-7Nb alloy, which is particularly prominent in biomedical applications. The concept of the study was built on examining the relationship between surface roughness (Ra) and laser processing parameters on engraved surfaces using 100 W laser marking machine. The parameter combinations used in this work are distinct from those found in the current literature about the micro-engraving capabilities of Ti-6Al-7Nb alloy.

2. Experimental Procedure

The Ti-6Al-7Nb alloy was used in the experimental research. Engraving with laser beam-aided machining (LAM) operations were conducted on the circular samples with a diameter of 16 mm. The laser marking machine utilized in this study was equipped with a ytterbium-doped fiber laser capable of generating an output power of up to 100 W (see Figure 1). This machine was employed to carry out laser engraving tasks for the test samples. During the experimental phase, the laser beam was precisely focused at a distance of 369 mm from the workpiece's surface. The standard engraving size was determined as a square measuring 12 mm by 12 mm. The parameters employed for LAM applications included power level (P %), scanning speed (SS), and scanning direction (SD). Every gravure was subjected to six repetitions based on the experimental combinations outlined in Table 1. The experiments were conducted under ambient conditions, at room temperature, without introducing additional gases.

The effectiveness of the parameters for engraved surfaces was analyzed using surface roughness and surface chemistry. The measurement of average surface roughness, denoted as Ra, was employed to assess the surface quality resulting from the laser engraving process. The measurement of surface roughness on the engraved surface was conducted using Mitutoyo (Surftest SJ-400). A total of six surface roughness measurements were conducted after the application of laser engraving to evaluate the characteristics of the surface. Analyses using energy-dispersive X-ray spectroscopy (EDX) and scanning electron microscopy (FEI-Quanta FEG 450) were performed on the engraved surface to examine its chemical composition and topography.

Figure 1. Laser marking machine-100 W

3. Results and Discussion

The present study investigates the surface engraving of the Ti-6Al-7Nb alloy using a laser beam. The experiment explores the effects of 18 distinct engraving conditions, which are determined by varying the scanning direction, laser power level (%), and scanning speed parameters. The following sections present the experimental results and evaluations.

3.1. Surface topography

The SEM analysis of the engraved samples subsequent to the laser micro-engraving procedure revealed the presence of a chaotic surface structure (see Figure 2). Figures 2 and 3 illustrate the observable existence of material residuals in particle and layer forms that occurred with forcefully propelled and spattered materials into the immediate vicinity of craters. Spattered materials in the form of layers and particles are concentrated in and near the grooves and extend beyond them. It is evident that these formations exhibit a high degree of efficacy in forming the surface topography. Using LAM technology on the surface of metallic materials produces debris such as drops, slags, spatter layers, and groove rim forms, substantially modifying the surface topography. The scanning direction is paramount in determining the beam's movement path. It has a significant effect on the surface topography by affecting the orientation of metal debris. As a result of the detailed examination of Figure 3, it was determined that there are cracks in different forms on the engraved surfaces. The occurrence of cracks

during the laser engraving process is considered to be influenced by the non-uniform thermal stresses and the rapid cycles of melting and resolidification, as reported elsewhere [26-28].

Table 1. Experimental setup and surface roughness measurement results

No	Scanning Direction (°)	Power Level (%)	Scanning Speed (mm/s)	Ra (µm)
L-1	45	60	200	17.1
L-2	45	60	450	14.2
L-3	45	60	700	9.9
L-4	45	90	200	23.2
L-5	45	90	450	22
L-6	45	90	700	17.3
L-7	90	60	200	16.6
L-8	90	60	450	14.3
L-9	90	60	700	7.5
L-10	90	90	200	22
L-11	90	90	450	21.6
L-12	90	90	700	16.6
L-13	45/90	60	200	19
L-14	45/90	60	450	18.7
L-15	45/90	60	700	16.9
L-16	45/90	90	200	22.7
L-17	45/90	90	450	22.6
L-18	45/90	90	700	20.4

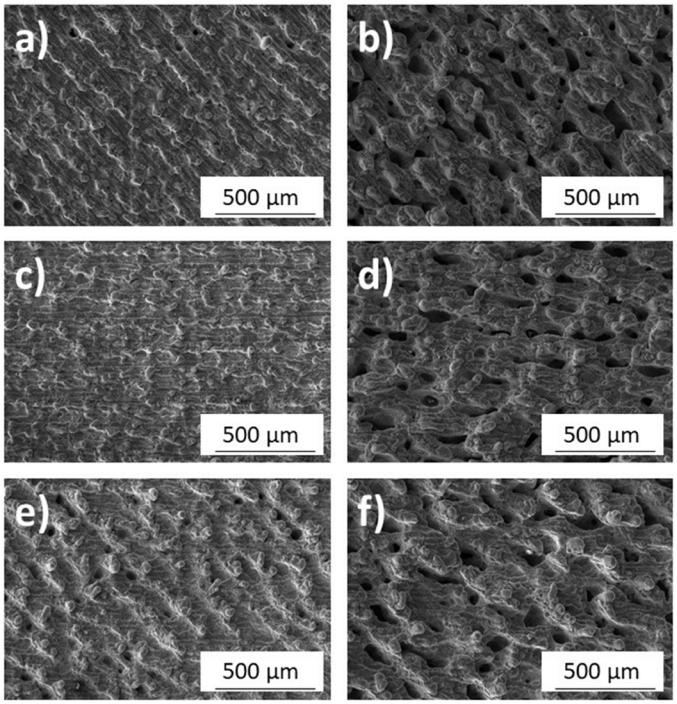

Figure 2. SEM images of the engraved samples: a) L-3; b) L-6; c) L-9; d) L-12; e) L-15; f) L-18

Figure 4 depicts the representative images of the elemental mapping of engraved surfaces. The phenomenon of plasma formation is observed when metal is exposed to laser beams. The occurrence of recoil pressure results in the displacement of the liquid metal present in the cavity after the vaporization stage, leading to its movement away from the cavity [29]. This mechanism is considered to have a distinct impact on the formation of surface topography and chemical structure. The distribution of elements on the engraved surface is visualized in different colors, as seen in Figure 4.

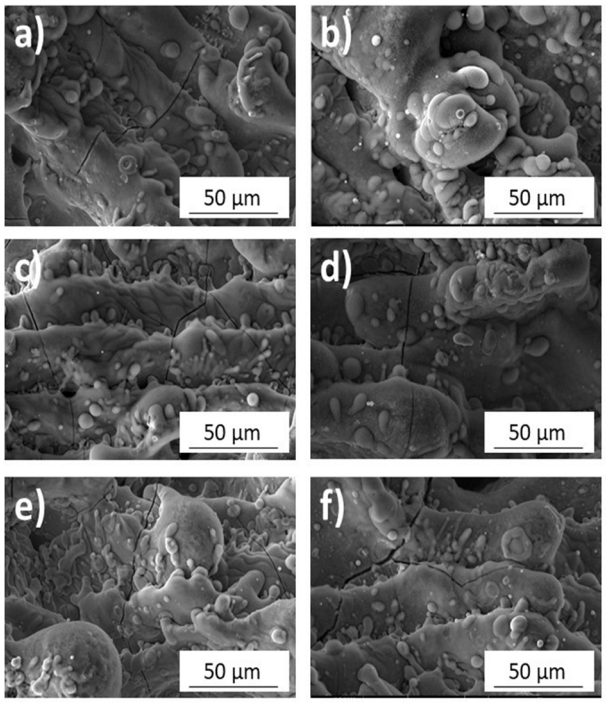

Figure 3. Surface formations of the engraved sample: a) L-3; b) L-6; c) L-9; d) L-12; e) L-15; f) L-18

3.2. The Impact of Parameters on Surface Roughness

Table 1 presents the findings of the surface roughness measurements conducted to ascertain the impact of the parameters on the surface roughness. Based on the data presented in Table 1, the primary impacts of the parameters on Ra were analyzed and presented in Figure 5. According to the mean surface roughness values in Figure 5, the highest and lowest surface roughness values are achieved when the scanning direction is adjusted at 45°/90° and 90°, respectively. Conversely, the scanning direction resulting in the highest and lowest surface roughness involves moving the beam at 45° and 90°, respectively (Table 1). Power is a fundamental parameter that quantifies the energy density per unit area. A phenomenon is that, at a constant frequency, the energy of a laser pulse exhibits an upward trend as the pulse power is increased. The relation for laser pulse energy is given in Eq. 1 [30].

$$Laser\ Pulse\ Energy\ (Joules) = \left(\frac{Average\ Power\ (Watts)}{Frequency\ (Hz)}\right) \quad (1)$$

For the two different power levels (%) selected within the scope of this study, the highest laser pulse energy value is reached with a high power level of 90%. As a result of the increase in the laser pulse energy, a high amount of material vaporization occurs, after which a rough surface is reached. Upon examination of Figure 5, it becomes evident that there is a positive correlation between the power

level (%) and the mean surface roughness, indicating that as the power level (%) increases, the mean surface roughness also increases. The surface roughness values ranged from 7.5 µm to 23.2 µm, with the lowest value observed at a power level of 60% and the highest at a power level of 90% (Table 1).

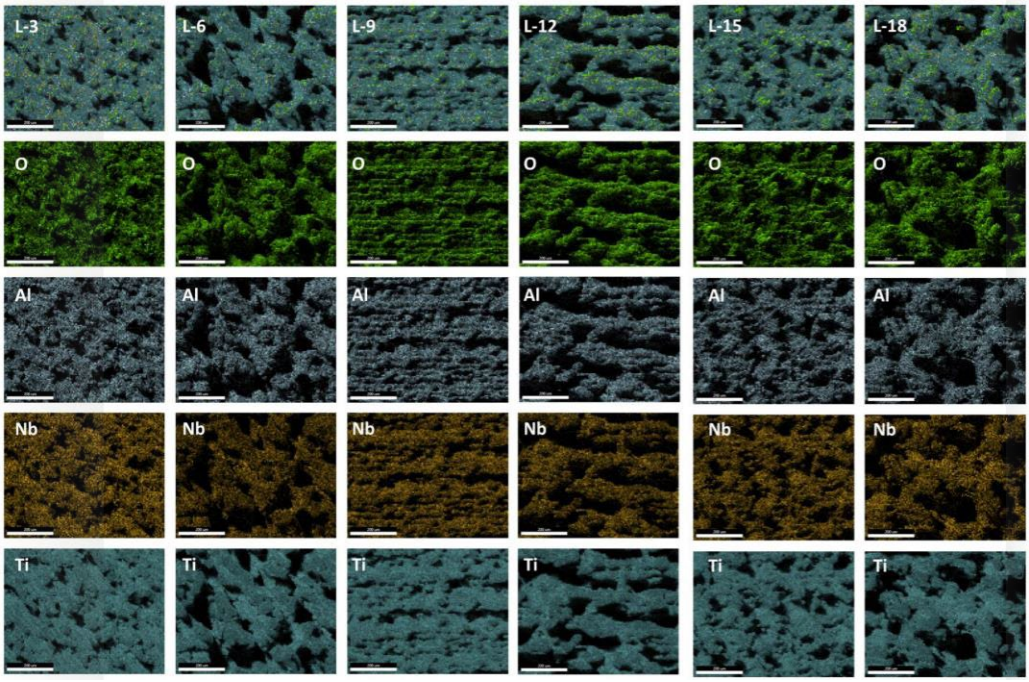

Figure 4. Representative images of elemental mapping of engraved surfaces for L-3, L6, L9, L-12, L15 and L18 specimens

The relationship between scanning speed and mean surface roughness is demonstrated in Figure 5. It has been ascertained that an increase in scanning speed is associated with a discernible trend toward a reduction in surface roughness, as reported elsewhere [28, 31-35]. This phenomenon's observed impact was found to be particularly notable within the range of scanning speeds spanning from 450 mm/s to 700 mm/s. The term "scanning speed" pertains to the velocity at which the laser beam moves in the predetermined scanning direction. This speed impacts the degree of overlap between successive laser beams. The overlap of the laser beams in a specific direction is expressed as pulse overlap; the amount of pulse overlap is calculated by Eq. 2 [36]. It is clear that the frequency also has a significant effect on the pulse overlap ratio, such as the scanning speed for a fixed pulse diameter.

$$O_P\ (\%) = \left(1 - \frac{scan\ speed}{laser\ beam\ diameter\ x\ frequency}\right) x100 \tag{2}$$

When a constant frequency value is used, resulting in an overlap, a reduction in scanning speed tends to increase the degree of pulse overlap. An increase in the degree of overlap per unit length leads to a rise in the area affected by the energy density and, as a result, an increase in the amount of evaporated materials and residual debris. The maximum surface roughness observed was 23.2 µm, related to the lowest scanning speed of 200 mm/s (Table 1). The scanning speed of 700 mm/s resulted in a minimum surface roughness of 7.5 µm (Table 1).

Interaction plots taking into account the average surface roughness and the relationship of the parameters with the surface roughness are shown in Figure 6. When the effect of scanning direction and power level (%) interaction is examined, all scanning strategies reveal a similar trend. Nevertheless, it becomes evident that the scanning strategies at 45° and 90° yield similar outcomes. When analyzing the

impact of the interaction between scanning direction and scanning speed, it is observed that all scanning strategies, namely 90°, 45°, and 45°/90°, exhibit a comparable effect. The experimental data suggests that the increase in scanning speed is associated with a decrease in surface roughness. The relationship between scanning speed and surface roughness is characterized by a consistent reduction in surface roughness as scanning speed increases, following a linear trend. When the effect of the interaction of the power level (%) with the scanning speed on the mean surface roughness is examined, it is seen that all power levels (%) for each scanning speed reveal a different effect on the surface roughness. It has been determined that an increase in scan speed is associated with a decrease in mean surface roughness for two power levels (%).

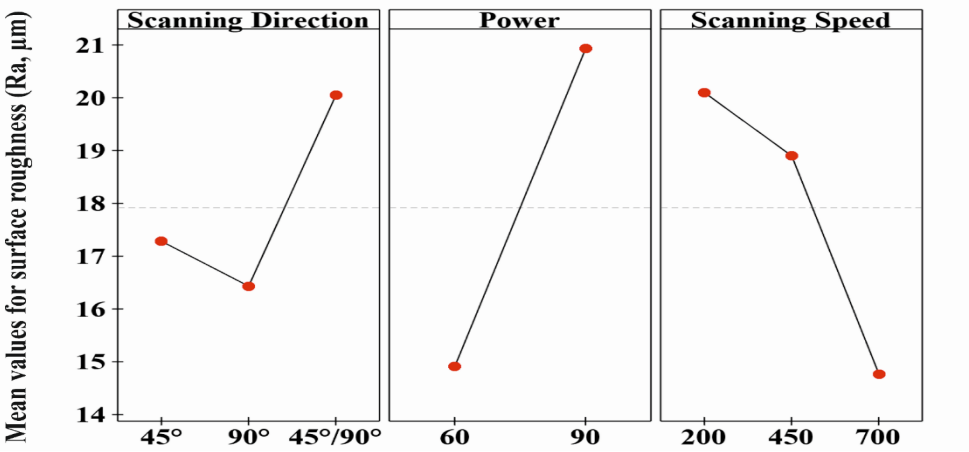

Figure 5. The primary impacts of the parameters on Ra

The analysis of variance (ANOVA) was conducted to statistically investigate the impact of each parameter on the surface roughness. The statistical data results are given in Table 2. The statistical significance of each parameter was assessed by examining the p-value. If the p-value was found to be less than 0.05, the corresponding parameter was determined to be statistically significant. Otherwise, the parameter is considered insignificant if the p-value exceeds 0.05. Upon examination of the p-values presented in Table 2, it is observed that the p-value for all parameters is less than 0.05. This finding suggests that every parameter exerts a statistically significant influence on the surface roughness. The calculated values of the parameter effects on surface roughness were also determined. Accordingly, power level (%) has the highest effect on surface roughness at 49.0%, scanning speed has the effect on surface roughness with a ratio of 28.2%, and scanning direction with a ratio of 12.9%.

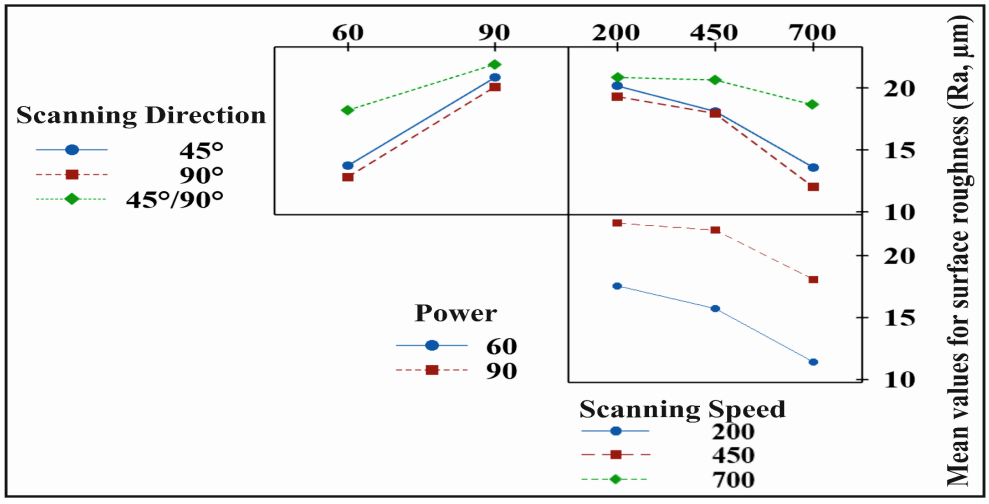

Figure 6. The interaction graphs of the parameters

Table 2. ANOVA results for surface roughness (Ra)

Source	df	Adj SS	F-Value	p-Value	Percentage Contribution
Scanning Direction	2	42.91	7.86	0.007	12.9
Power Level (%)	1	163.20	59.79	0.000	49.0
Scanning Speed	2	93.94	17.21	0.000	28.2
Error	12	32.76			9.8
Total	17	332.81			

3.3. Surface chemical composition

Table 3 presents the proportions of the identified elements on the surface that underwent laser engraving. The results presented in this section comprise the Energy Dispersive X-ray (EDX) analysis that was performed on the designated region (Figure 7). The first comparison was made for the oxygen (O) concentration of the engraved surfaces. After conducting a comparison of the oxygen contents on the selected surfaces, it was observed that the engraved sample L-3 displayed the lowest oxygen content, detected at 31.27%. The oxygen contents in increasing order for L-3, L-9, L-15, L-18, L-6, and L-12 surfaces is 31.27%, 35.61%, 35.73%, 40.42%, 41.55%, and 44.21%, respectively. The detected presence of oxygen in the analysis is hypothesized to originate from metal oxides formed throughout and subsequent to the relevant process, as reported elsewhere [34, 35]. The respective proportions of carbon content in L-3, L-6, L-9, L-12, L-18, and L-15 are measured to be 2.51%, 2.72%, 2.79%, 3.10%, 3.13%, and 3.50%, respectively. The presence of carbon that has been detected could potentially be ascribed to the contamination of carbon rather than being a result of the laser surface treatment procedures as reported elsewhere [32, 37, 38].

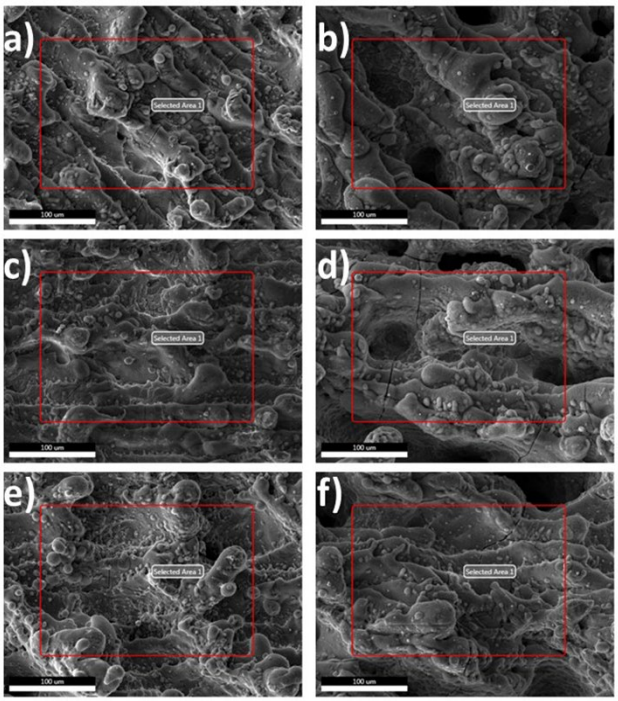

Figure 7. Selected areas for SEM-EDS analysis on laser engraved specimens: a) L-3; b) L-6; c) L-9; d) L-12; e) L-15; f) L-18

Table 3. The results of SEM-EDS on engraved surfaces

	Elements' ratios (wt.%)				
Nos.	**C**	**O**	**Al**	**Nb**	**Ti**
L-3	2.51	31.27	3.32	3.35	59.56
L-6	2.72	41.55	3.38	2.46	49.89
L-9	2.79	35.61	3.15	3.50	54.95
L-12	3.10	44.21	3.30	2.36	47.04
L-15	3.50	35.73	3.00	2.86	54.91
L-18	3.13	40.42	3.44	2.83	50.18

4. Conclusion

Surface roughness values ranged from 7.5 µm to 23.2 µm; the values of 7.5 µm and 23.2 µm corresponded to the 60% and 90% power levels, respectively. The highest surface roughness value was observed when the scanning direction was set at an angle of 45°, and the scanning speed was set to 200 mm/s. In contrast, the surface roughness value was found to be the lowest when the scanning speed was adjusted to 700 mm/s and the scanning direction was set at an angle of 90°. Notably, the mean surface roughness results indicate that the scanning direction of 45°/90° yields the highest mean surface roughness, whereas the scanning direction of 90° yields the lowest. Surface roughness tends to decrease with increasing scanning speed. However, as power level (%) increased, so did surface roughness. The study reveals that the scanning speed has a significant impact of 28.2% on surface roughness, whereas the scanning direction has a comparatively lower influence of 12.9%. The variable of power level (%) demonstrates the most significant impact on surface roughness, explaining 49% of the observed variability. By eliminating the challenges associated with cutting tools, laser micro-engraving of Ti-6Al-7Nb alloy is evaluated to be an alternative to conventional manufacturing techniques for the precision production of components in the biomedical industry.

5. Ethics committee approval and conflict of interest statement

Obtaining ethics committee permission for the prepared article is unnecessary. Additionally, there is no conflict of interest with any person/institution.

References

[1] Bakhtiyari AN, Wang Z, Wang L, Zheng H. A review on applications of artificial intelligence in modeling and optimization of laser beam machining, Optics & Laser Technology 2021; 135: 106721.
[2] Rao RV, Kalyankar VD. Optimization of modern machining processes using advanced optimization techniques: a review, The International Journal of Advanced Manufacturing Technology 2014; 73: 1159-1188.
[3] Brousseau EB, Dimov SS, Pham DT. Some recent advances in multi-material micro- and nano-manufacturing, The International Journal of Advanced Manufacturing Technology 2010; 47: 161-180.
[4] Saklakoglu IE, Kasman S. Investigation of micro-milling process parameters for surface roughness and milling depth, The International Journal of Advanced Manufacturing Technology 2011; 54: 567-578.
[5] Dubey AK, Yadava V. Laser beam machining—A review, International Journal of Machine Tools and Manufacture 2008; 48: 609-628.

[6] Parandoush P, Hossain A. A review of modeling and simulation of laser beam machining, International Journal of Machine Tools and Manufacture 2014; 85: 135-145.
[7] Romoli L. Flattening of surface roughness in ultrashort pulsed laser micro-milling, Precision Engineering 2018; 51: 331-337.
[8] Ramesh S, Karunamoorthy L, Palanikumar K. Measurement and analysis of surface roughness in turning of aerospace titanium alloy (gr5), Measurement 2012; 45: 1266-1276.
[9] Peters M, Kumpfert J, Ward CH, Leyens C. Titanium Alloys for Aerospace Applications, Advanced Engineering Materials 2003; 5: 419-427.
[10] Boyer RR. An overview on the use of titanium in the aerospace industry, Materials Science and Engineering: A 1996; 213: 103-114.
[11] Ozan S, Lin J, Li Y, Ipek R, Wen C. Development of Ti–Nb–Zr alloys with high elastic admissible strain for temporary orthopedic devices, Acta Biomaterialia 2015; 20: 176-187.
[12] Ozan S, Lin J, Li Y, Wen C. New Ti-Ta-Zr-Nb alloys with ultrahigh strength for potential orthopedic implant applications, Journal of the Mechanical Behavior of Biomedical Materials 2017; 75: 119-127.
[13] Lin J, Ozan S, Li Y, Ping D, Tong X, Li G, Wen C. Novel Ti-Ta-Hf-Zr alloys with promising mechanical properties for prospective stent applications, Scientific Reports 2016; 6: 37901.
[14] Munir K, Lin J, Wright PFA, Ozan S, Li Y, Wen C. Mechanical, corrosion, nanotribological, and biocompatibility properties of equal channel angular pressed Ti-28Nb-35.4Zr alloys for biomedical applications, Acta Biomaterialia 2022; 149: 387-398.
[15] Lin J, Ozan S, Munir K, Wang K, Tong X, Li Y, Li G, Wen C. Effects of solution treatment and aging on the microstructure, mechanical properties, and corrosion resistance of a β type Ti–Ta–Hf–Zr alloy, RSC Advances 2017; 7: 12309-12317.
[16] Ozan S, Munir K, Biesiekierski A, Ipek R, Li Y, Wen C. 1.3.3A - Titanium Alloys, Including Nitinol. *In* Wagner W.R., Sakiyama-Elbert S.E., Zhang G., Yaszemski M.J. (ed), Biomaterials Science (Fourth Edition). Academic Press, Elsevier 2020; Cambridge, 229-247.
[17] Jawaid A, Che-Haron CH, Abdullah A. Tool wear characteristics in turning of titanium alloy Ti-6246, Journal of Materials Processing Technology 1999; 92-93: 329-334.
[18] Alahmari AM, Darwish S, Ahmed N. Laser beam micro-milling (LBMM) of selected aerospace alloys, The International Journal of Advanced Manufacturing Technology 2016; 86: 2411-2431.
[19] Bai H, Zhong L, Kang L, Liu J, Zhuang W, Lv Z, Xu Y. A review on wear-resistant coating with high hardness and high toughness on the surface of titanium alloy, Journal of Alloys and Compounds 2021; 882: 160645.
[20] Courant B, Hantzpergue JJ, Benayoun S. Surface treatment of titanium by laser irradiation to improve resistance to dry-sliding friction, Wear 1999; 236: 39-46.
[21] Niinomi M. Mechanical biocompatibilities of titanium alloys for biomedical applications, Journal of the Mechanical Behavior of Biomedical Materials 2008; 1: 30-42.
[22] Niinomi M. Recent research and development in titanium alloys for biomedical applications and healthcare goods, Science and Technology of Advanced Materials 2003; 4: 445.
[23] Challa VSA, Mali S, Misra RDK. Reduced toxicity and superior cellular response of preosteoblasts to Ti-6Al-7Nb alloy and comparison with Ti-6Al-4V, Journal of Biomedical Materials Research Part A 2013; 101A: 2083-2089.
[24] Semlitsch M, Staub F, Weber H. Titanium-Aluminium-Niobium Alloy, Development for Biocompatible, High Strength Surgical Implants - Titan-Aluminium-Niob-Legierung, entwickelt für körperverträgliche, hochfeste Implantate in der Chirurgie, Biomedical Engineering/ Biomedizinische Technik 1985; 30: 334-339.
[25] Costa TBd, Pereira RBD, Lauro CH, Brandão LC, Davim JP. Statistical learning and optimization of the helical milling of the biocompatible titanium Ti-6Al-7Nb alloy, The International Journal of Advanced Manufacturing Technology 2023; 125: 1789–1813
[26] Eghbali N, Naffakh-Moosavy H, Sadeghi Mohammadi S, Naderi-Manesh H. The influence of laser frequency and groove distance on cell adhesion, cell viability, and antibacterial characteristics of Ti-6Al-4V dental implants treated by modern fiber engraving laser, Dental Materials 2021; 37: 547-558.

[27] Manninen M, Hirvimäki M, Poutiainen I, Salminen A. Effect of Pulse Length on Engraving Efficiency in Nanosecond Pulsed Laser Engraving of Stainless Steel, Metallurgical and Materials Transactions B 2015; 46: 2129-2136.
[28] Kasman Ş, Uçar İC, Ozan S. Investigation into the effects of laser texturing parameters on surface properties of Ti-6Al-4V ELI biomedical alloy, Journal of the Brazilian Society of Mechanical Sciences and Engineering 2023; 45: 231.
[29] Wang Y, Zhang M, Li K, Hu J. Study on the surface properties and biocompatibility of nanosecond laser patterned titanium alloy, Optics & Laser Technology 2021; 139: 106987.
[30] Hribar L, Gregorčič P, Senegačnik M, Jezeršek M. The Influence of the Processing Parameters on the Laser-Ablation of Stainless Steel and Brass during the Engraving by Nanosecond Fiber Laser, Nanomaterials 2022; 12(2): 232.
[31] Kasman Ş, Ozan S. Machinability of AA 2024 aluminum alloy by fiber laser engraving process, Materialwissenschaft und Werkstofftechnik 2023; 54: 646-655.
[32] Kasman Ş, Uçar IC, Ozan S. The Effects of Laser Surface Texturing Parameters on the Surface Characteristics of Biomedical-Grade Stainless Steel, Journal of Materials Engineering and Performance 2023; DOI: 10.1007/s11665-023-08374-7
[33] Kasman Ş, Uçar İC, Ozan S. Laser Surface Texturing of Co–Cr–Mo Alloy for Biomedical Applications: A Case Study for the Effects of Process Parameters on Surface Properties, Journal of Bionic Engineering 2023; 20: 1967-1984.
[34] Kasman Ş, Uçar İC, Ozan S. Investigation of laser surface texturing parameters of biomedical grade Co-Cr-Mo alloy, The International Journal of Advanced Manufacturing Technology 2023; 125: 4271-4291.
[35] Ozan S, Bilgin A, Kasman Ş. Laser textured Ti-6Al-7Nb alloy for biomedical applications: An investigation of texturing parameters on surface properties, Proceedings of the Institution of Mechanical Engineers, Part H: Journal of Engineering in Medicine 2023; 237(10):1139-1153
[36] Menci G, Demir AG, Waugh DG, Lawrence J, Previtali B. Laser surface texturing of β-Ti alloy for orthopaedics: Effect of different wavelengths and pulse durations, Applied Surface Science 2019; 489: 175-186.
[37] Hočevar M, Šetina Batič B, Godec M, Kononenko V, Drobne D, Gregorčič P. The interaction between the osteosarcoma cell and stainless steel surface, modified by high-fluence, nanosecond laser pulses, Surface and Coatings Technology 2020; 394: 125878.
[38] Purnama A, Furlan V, Dessi D, Demir AG, Tolouei R, Paternoster C, Levesque L, Previtali B, Mantovani D. Laser surface texturing of SS316L for enhanced adhesion of HUVECs, Surface Engineering 2020; 36: 1240-1249.